Two distinct voltage-sensing domains control voltage sensitivity and kinetics of current activation in Ca_V1.1 calcium channels

Petronel Tuluc,[1]* Bruno Benedetti,[2]* Pierre Coste de Bagneaux,[2] Manfred Grabner,[3] and Bernhard E. Flucher[2]

[1]Department of Pharmacology and Toxicology, Institute of Pharmacy, University of Innsbruck, A-6020 Innsbruck, Austria
[2]Department of Physiology and Medical Physics and [3]Department of Medical Genetics, Molecular and Clinical Pharmacology, Medical University Innsbruck, A-6020 Innsbruck, Austria

Alternative splicing of the skeletal muscle Ca_V1.1 voltage-gated calcium channel gives rise to two channel variants with very different gating properties. The currents of both channels activate slowly; however, insertion of exon 29 in the adult splice variant Ca_V1.1a causes an ∼30-mV right shift in the voltage dependence of activation. Existing evidence suggests that the S3–S4 linker in repeat IV (containing exon 29) regulates voltage sensitivity in this voltage-sensing domain (VSD) by modulating interactions between the adjacent transmembrane segments IVS3 and IVS4. However, activation kinetics are thought to be determined by corresponding structures in repeat I. Here, we use patch-clamp analysis of dysgenic (Ca_V1.1 null) myotubes reconstituted with Ca_V1.1 mutants and chimeras to identify the specific roles of these regions in regulating channel gating properties. Using site-directed mutagenesis, we demonstrate that the structure and/or hydrophobicity of the IVS3–S4 linker is critical for regulating voltage sensitivity in the IV VSD, but by itself cannot modulate voltage sensitivity in the I VSD. Swapping sequence domains between the I and the IV VSDs reveals that IVS4 plus the IVS3–S4 linker is sufficient to confer Ca_V1.1a-like voltage dependence to the I VSD and that the IS3–S4 linker plus IS4 is sufficient to transfer Ca_V1.1e-like voltage dependence to the IV VSD. Any mismatch of transmembrane helices S3 and S4 from the I and IV VSDs causes a right shift of voltage sensitivity, indicating that regulation of voltage sensitivity by the IVS3–S4 linker requires specific interaction of IVS4 with its corresponding IVS3 segment. In contrast, slow current kinetics are perturbed by any heterologous sequences inserted into the I VSD and cannot be transferred by moving VSD I sequences to VSD IV. Thus, Ca_V1.1 calcium channels are organized in a modular manner, and control of voltage sensitivity and activation kinetics is accomplished by specific molecular mechanisms within the IV and I VSDs, respectively.

INTRODUCTION

Voltage-gated calcium channels (Ca_V's) control numerous important functions of excitable cells, including muscle contraction, hormone and neurotransmitter secretion, and activity-dependent gene regulation. According to this variety of cell functions, the different Ca_V isoforms and splice variants greatly vary in their voltage dependence and current kinetics (Lipscombe et al., 2013). Of all the Ca_V isoforms, the adult splice variant of the skeletal muscle calcium channel (Ca_V1.1a) has the most depolarized voltage dependence and the slowest current kinetics. In contrast, the embryonic splice variant Ca_V1.1e, which lacks the alternatively spliced exon 29, activates at much less depolarized membrane potentials (Tuluc et al., 2009).

In skeletal muscle, Ca_V1.1 primarily functions as the voltage sensor of excitation-contraction (EC) coupling (Melzer et al., 1995). For this signaling process, calcium influx through the Ca_V1.1 channel is dispensable, and it is questionable whether in the duration of a brief skele-

tal muscle action potential calcium influx through Ca_V1.1a is activated at all (Armstrong et al., 1972; Rios and Brum, 1987). In fact, calcium influx during skeletal muscle EC coupling may even be harmful, as aberrant expression of the embryonic, calcium-conducting Ca_V1.1e isoform in adult mice and humans is linked to muscle weakness and disease (Tang et al., 2012; Santoro et al., 2014; Sultana et al., 2016). Therefore, the molecular mechanisms regulating calcium currents in Ca_V1.1 are of high physiological and pathological importance.

The pore-forming Ca_V α_1 subunits are the product of a single gene composed of four homologous repeats (I–IV), each containing six transmembrane helices (S1–S6; Catterall, 2011). S5, S6, and the connecting pore loop of the four repeats together comprise the channel pore with the selectivity filter and the activation gate. S1 through S4 of each repeat make up the voltage-sensing domains (VSDs). The S4 helices contain four to five positive charges (argi-

The Journal of General Physiology

nines and lysines) that in response to membrane depolarization move across the membrane and thereby initiate the allosteric opening of the channel pore. In analogy with the more in-depth-studied VSDs of potassium and sodium channels, it is assumed that during the gating process the positively charged amino acids in S4 sequentially interact with two negatively charged (aspartate and glutamate) and one polar amino acid (phenylalanine) in the S2 and S3 helices, called the charge transfer center (Tao et al., 2010). The movement of these voltage sensors upon depolarization determines the activation properties of voltage-gated cation channels, and drugs interfering with the voltage sensor movement modify channel gating (Gur et al., 2011; Wang et al., 2011).

Recently, we discovered the molecular mechanism by which the voltage dependence of channel activation is regulated in $Ca_V1.1$ (Tuluc et al., 2016). Incorporation of the alternatively spliced exon 29 into the extracellular loop connecting transmembrane helices S3 and S4 of the IV VSD shifts the voltage dependence of activation by ~30 mV in the depolarizing direction (Tuluc et al., 2009). This inhibiting action of exon 29 critically depends on the two outermost arginines (R1 and R2) in IVS4 and on an aspartate (D4) near the extracellular side of the IVS3 helix (Tuluc et al., 2016). Based on structure modeling and mutagenesis data, we proposed a model according to which transient interactions of R1 and R2 with the counter charge D4 are important for regular voltage sensing of the IV VSD of $Ca_V1.1e$, and inclusion of exon 29 in the IVS3–S4 linker in $Ca_V1.1a$ somehow interferes with this interaction, causing the observed reduction of voltage sensitivity (Fig. 1 B).

Here, we used site-directed mutagenesis and domain swapping between the I and IV VSDs to address the question as to whether exon 29 by itself has the potential of curtailing $Ca_V1.1$ currents, whether the proposed D4–R1/R2 interaction is specific to the IV VSD or can also function in the I VSD, and how regulation of voltage dependence of activation relates to regulation of activation kinetics. Our results extend and refine our original model by demonstrating that IVS4 is fundamentally different from the voltage sensor in the I repeat, such that IVS4 critically requires the transient interactions with the additional counter charge D4. This sophistication of the IV VSD makes it receptive to modulation by alternative splicing of IVS3–S4 linker. However, neither the IVS3–S4 linker containing exon 29 nor the IVS3 helix containing D4 by themselves or together have the potential to regulate voltage dependence of activation. Moreover, our data demonstrate that regulation of voltage dependence and kinetics of current activation are spatially separated in the I and IV repeats, respectively, and are functionally independent of each other.

MATERIALS AND METHODS

Expression plasmids

The $Ca_V1.1$ channel chimeras were generated using splicing by overhang extension PCR into the GFP-α_{1S}, GFP-α_{1S}–ΔE29, or GFP-α_{1C} plasmids previously described (Tuluc et al., 2007, 2009) and verified by sequencing performed by Eurofins Genomis. For the chimeras where sequences of the IV VSD were transferred into the I VSD, a three-fragment PCR was generated with flanking primers downstream of the SalI enzyme restriction site and upstream of the EcoRI restriction site. The obtained PCR fragments were cloned into the GFP-α_{1S}–ΔE29-containing plasmid using SalI and EcoRI restriction sites. The same restriction sites were used to clone the cardiac S3 and S3–S4 linker into $Ca_V1.1a$ or $Ca_V1.1e$ variants. For the chimeras containing sequences of the I repeat in the IV repeat or for the $Ca_V1.1a$-$L_{1212/L1215}$N chimera, a three-fragment PCR or two-fragment PCR, respectively, was generated with the flanking primers upstream of the XhoI site and downstream of the BglII site. The same sites were used to clone the obtained PCR fragment into the GFP-α_{1S}– or GFP-α_{1S}–ΔE29-containing plasmids. Table S1 contains the full list of the cloning primers used to generate the PCR fragments.

Myotube cell culture and transfection

Myoblasts of the dysgenic (*mdg/mdg*) cell line GLT were transfected 4 d after plating using FuGENE-HD transfection reagent (Roche). Transfected myotubes, identified by GFP fluorescence, were analyzed between 8 and 10 d in culture (Tuluc et al., 2007). GLT myotubes endogenously express the auxiliary $\alpha_2\delta$-1, β_{1a}, and γ_1 calcium channel subunits as well as STAC3 and the ryanodine receptor, enabling proper functional incorporation of the channel constructs in the triad junction (Rios and Brum, 1987; Tanabe et al., 1988; Flucher et al., 2005).

Electrophysiology and data analysis

Calcium currents were recorded with the ruptured whole-cell patch-clamp technique in voltage-clamp mode using an Axopatch 200B amplifier (Axon Instruments). Patch pipettes (borosilicate glass; Harvard Apparatus) were filled with (mM) 145 Cs-aspartate, 2 $MgCl_2$, 10 HEPES, 0.1 Cs-EGTA, and 2 Mg-ATP (pH 7.4 with CsOH) and had a resistance between 1.5 and 3 MΩ. For the recording of the calcium currents, the myotubes were bathed in solution containing (mM) 10 $CaCl_2$, 145 tetraethylammonium chloride, and 10 HEPES (pH 7.4 with tetraethylammonium hydroxide). Data acquisition and command potentials were controlled by pCLAMP software (version 8.0; Axon Instruments); analysis was performed using Clampfit 8.0 (Axon Instruments) and SigmaPlot 8.0 (SPSS Science) software. The current-voltage

Structural determinants of $Ca_V1.1$ gating | Tuluc et al.

Table 1. **Voltage of half-maximal activation ($V_{1/2}$) and current density at maximal activation (I_{peak})**

Constructs	$V_{1/2}$ (mV)				I_{peak} (pA/pF)				N
	Mean	SD	SEM	P	Mean	SD	SEM	P	
$Ca_V1.1a$	34.8	4.9	0.9	na,†††	1.8	0.7	0.1	na,†††	31
$Ca_V1.1e$	6.7	5.7	1.0	***,na	10.5	4.3	0.7	***,na	30
$Ca_V1.1a\text{-}L_{1212/1215}N$	23.0	5.1	1.5	***,†††	4.8	2.4	0.7	ns,ns	12
$Ca_V1.1e\text{-}L_I$	11.7	4.5	0.9	***,†	12.5	6.6	1.3	***,ns	25
$Ca_V1.1e\text{-}L4_I$	36.4	8.3	3.1	ns,†††	0.6	0.2	0.1	ns,†††	7
$Ca_V1.1e\text{-}3L_I$	12.4	3.8	1.4	***,ns	5.8	2.3	0.8	ns,ns	7
$Ca_V1.1a\text{-}CS_I$	31.3	4.0	1.1	ns,†††	2.3	1.8	0.5	ns,†††	12
$Ca_V1.1e\text{-}CS_I$	−1.6	6.4	2.1	***,††	12.0	8.3	2.7	***,ns	9
$Ca_V1.1e\text{-}L_I\text{-}3L_{IV}$	36.1	5.7	1.5	ns,†††	2.1	1.2	0.3	ns,†††	14
$Ca_V1.1e\text{-}L_I\text{-}L4_{IV}$	5.2	3.3	0.9	***,ns	9.6	4.3	1.2	***,ns	12
$Ca_V1.1e\text{-}L_I\text{-}L_{IV}$	21.2	7.3	1.7	***,†††	7.0	3.1	0.7	***,ns	18
$Ca_V1.1e\text{-}L_I\text{-}3L4_{IV}$	10.6	5.3	2.0	***,ns	8.7	4.5	1.7	**,ns	7

Numerical values represent mean, SD, SEM, and number of samples (N). Statistical differences between mutants, chimeras, and $Ca_V1.1a$ or $Ca_V1.1e$ were determined with one-way ANOVA, followed by a Bonferroni multiple comparison test. Significant differences against $Ca_V1.1a$ are indicated as **, P < 0.001; ***, P < 0.0001. Differences against $Ca_V1.1e$ are indicated as †, P < 0.05; ††, P < 0.001; †††, P < 0.0001. ns, not significant (P < 0.05); na, not applicable.

dependence was fitted according to $I = G_{max} \cdot (V - V_{rev})/1(1 + \exp(-(V - V_{1/2})/k))$, where, G_{max} is the maximum conductance of the L-type calcium currents, V_{rev} is the extrapolated reversal potential of the calcium current, $V_{1/2}$ is the potential for half maximal conductance, and k is the slope. The conductance was calculated using $G = (-I * 1000)/(V - V_{rev})$, and its voltage dependence was fitted according to a Boltzmann distribution: $G = G_{max}/(1 + \exp(-(V - V_{1/2})/k))$. The statistical significance was calculated using the Mann–Whitney U test (see Tables 1 and 2).

Online supplemental material

Our supplemental material provides a figure (Fig. S1) displaying the relation between I_{peak} and $V_{1/2}$ of wild-type and mutated $Ca_V1.1$ channels and a table (Table S1) with the full list of the cloning primers used to generate the PCR fragments. Online supplemental material is available at http://www.jgp.org/cgi/content/full/jgp.201611568/DC1.

RESULTS

The structure of the IVS3–S4 linker is important for the control of voltage sensitivity and current density in $Ca_V1.1a$

Inclusion of the 19–amino acid sequence of exon 29 in the extracellular linker between transmembrane helices IVS3 and IVS4 shifts the channel voltage sensitivity of $Ca_V1.1$ by ~30 mV in the depolarizing direction (Tuluc et al., 2009). Recently, we demonstrated that a hitherto unnoticed interaction of oppositely charged

Table 2. **Time constants of current activation**

Constructs	Kinetics	Time constant (ms)			P	N
		Mean	SD	SEM		
$Ca_V1.1a$	$slow$	43.3	25.8	4.7	na,†††	30
	$fast$	7.4	3.6	0.6	na,ns	
$Ca_V1.1e$	$slow$	22.6	13.9	3.1	***,na	20
	$fast$	4.4	2.3	0.5	ns,na	
$Ca_V1.1a\text{-}L_{1212/1215}N$	$slow$	16.5	7.4	2.6	***,ns	8
	$fast$	4.5	2.6	0.9	ns,ns	
$Ca_V1.1e\text{-}L_I$		4.1	3.0	0.6	na	25
$Ca_V1.1e\text{-}L4_I$		2.7	1.3	0.5	ns	6
$Ca_V1.1e\text{-}3L_I$		4.1	1.6	0.6	ns	7
$Ca_V1.1a\text{-}CS_I$		3.3	0.9	0.3	ns	12
$Ca_V1.1e\text{-}CS_I$	$mono$	4.7	2.1	0.8	ns	7
$Ca_V1.1e\text{-}L_I\text{-}3L_{IV}$		4.0	1.9	0.5	ns	14
$Ca_V1.1e\text{-}L_I\text{-}L4_{IV}$		10.4	2.7	0.8	°°°	12
$Ca_V1.1e\text{-}L_I\text{-}L_{IV}$		4.1	1.6	0.4	ns	18
$Ca_V1.1e\text{-}L_I\text{-}3L4_{IV}$		2.6	0.7	0.2	ns	7

The activation of $Ca_V1.1a$, $Ca_V1.1e$, and $Ca_V1.1a\text{-}L_{1212/1215}N$ was fitted by a double-exponential function, whereas all other currents were best fitted with a mono-exponential function. Numerical values represent mean, SD, and SEM. Statistical differences between mutants, chimeras, and $Ca_V1.1a$ or $Ca_V1.1e$ were measured with one-way ANOVA, followed by a Bonferroni multiple comparison test. Significant differences against $Ca_V1.1a$ are indicated as ***, P < 0.0001. Differences against $Ca_V1.1e$ are indicated as †††, P < 0.0001. For mono-exponential time constants, differences against $Ca_V1.1e\text{-}L_I$ are indicated as °°°, P < 0.0001. ns, not significant (P < 0.05); na, not applicable.

residues in IVS3 and IVS4 is the critical determinant of $Ca_V1.1$ voltage sensitivity and that alternative splicing of the IVS3–S4 linker modulates this interaction (Fig. 1, A and B; Tuluc et al., 2016). If the specific structure of the IVS3–S4 linker causes the relative displacement of the adjacent transmembrane helices and thus perturbs the D4–R1/R2 interaction, changes of its structure should exert strong effects on voltage sensitivity. This prediction was tested by simultaneously mutating two leucines in the middle of the $Ca_V1.1a$ exon 29 to asparagine (L1212N and L1215N). Our original Rosetta models of the IVS3–S4 linker (Tuluc et al., 2016) and additional structure prediction tools (NPS@: Network Protein Sequence Analysis [Combet et al., 2000]) indicate that these leucines impart secondary structure (α-helix or β-sheet) and hydrophobicity to the extracellular loop, both of which are abolished by the double mutation (Fig. 1, A, C, and D).

This ($Ca_V1.1a$-$L_{1212/1215}N$) mutant and all other $Ca_V1.1$ constructs analyzed in the present study were expressed in dysgenic (α_{1S} null) myotubes of the GLT cell line (Powell et al., 1996). In these myotubes, $Ca_V1.1$ constructs are incorporated in functional channel complexes of triads and peripheral couplings and functionally reconstitute skeletal muscle EC coupling (Flucher et al., 2000; Kugler et al., 2004). An N-terminally fused eGFP aided in the selection of transfected myotubes for patch-clamp analysis. Transfected myotubes were voltage-clamped at a holding potential of −80 mV, and series of currents were recorded during 200-ms test pulses to potentials between −50 and 80 mV, increasing at 10-mV increments. Fig. 1 (E–G) shows representative current traces at the maximal test potential, the mean I-V curves, and the voltage dependence of fractional activation for the two splice variants ($Ca_V1.1a$ and $Ca_V1.1e$) and for the $Ca_V1.1a$-$L_{1212/1215}N$ mutant. As previously demonstrated (Tuluc et al., 2009; Benedetti et al., 2015), the two wild-type variants differ in that the embryonic splice variant $Ca_V1.1e$ lacking exon 29 activates at ~30 mV less depolarizing potentials and conducts several-fold higher current densities compared with the adult/classical $Ca_V1.1a$. The different current densities were independent of membrane expression of the channels. Both the magnitudes of gating currents and of depolarization-induced calcium transients were identical in myotubes expressing either one of the $Ca_V1.1$ variants (Tuluc et al., 2009). Mutation of the two leucines in exon 29 ($Ca_V1.1a$-$L_{1212/1215}N$) resulted in a 2.5-fold increase of current density and an 11.8-mV left shift of the voltage dependence of activation (P < 0.0001; Fig. 1, E–G; and Table 1). Therefore, interfering with the structure and hydrophobicity of the IVS3–S4 linker changed these gating properties in $Ca_V1.1a$ approximately half way in the direction of the splice variant lacking exon 29 ($Ca_V1.1e$). In contrast, the double leucine mutation had little effect on activation ki-

netics. As in the two wild-type splice variants ($Ca_V1.1a$ and $Ca_V1.1e$), current activation could best be fit with a double-exponential function (Caffrey, 1994; Avila and Dirksen, 2000; Obermair et al., 2005), and the time constants of the slow and fast components of $Ca_V1.1a$-$L_{1212/1215}N$ were similar to those of $Ca_V1.1e$ (Fig. 1, H and I; and Table 2). Thus, mutation of leucines 1212 and 1215 in the IVS3–S4 linker of $Ca_V1.1a$ qualitatively reproduces the effects on channel gating of exclusion of exon 29.

Control of voltage sensitivity and current amplitude can be transferred from the IV to the I VSD

To examine whether the IVS3–S4 linker including exon 29 by itself can modulate voltage sensitivity also in the context of a different VSD that does not contain the critical negatively charged amino acid (D4) in the transmembrane helix S3, we generated a channel chimera in which we inserted the IVS3–S4 linker including exon 29 into the corresponding position of the first repeat (Fig. 2 A). As this chimera was constructed in the background of the $Ca_V1.1e$ splice variant, exon 29 is lacking in the IV, but instead is present in the I repeat (Fig. 2 B). If intrinsic features of the IVS3–S4 linker were sufficient to limit current activation, the current properties of this chimera would be shifted from those of $Ca_V1.1e$ toward those of $Ca_V1.1a$, i.e., showing right-shifted voltage sensitivity of activation and reduced current amplitude. However, transferring the IVS3–S4 linker sequence to repeat I of $Ca_V1.1e$ ($Ca_V1.1e$-L_I) resulted in rapidly activating and partially inactivating calcium currents with otherwise unaltered gating properties (Fig. 2 C). The mean amplitude of the early current peak was equal to that of the starting construct $Ca_V1.1e$ (P = 0.2; Fig. 2 D), and most importantly, the voltage dependence of current activation was only minimally shifted relative to that of $Ca_V1.1e$ (Fig. 2 E and Table 1). Half-maximal voltage of activation ($V_{1/2}$) of $Ca_V1.1e$-L_I was 11.7 ± 0.9 mV; that is only 5 mV from that of $Ca_V1.1e$ ($V_{1/2}$ = 6.7 ± 1.0 mV; P < 0.05) but more than −20 mV from that of $Ca_V1.1a$ (34.8 ± 0.9 mV; P < 0.0001). Thus, the IVS3–S4 linker sequence, which regulates voltage sensitivity of the IV VSD, does not exert a modulatory action on the I VSD.

To further examine whether also in the context of the I VSD exon 29 requires the critical aspartate D4 in the S3 helix to exert its limiting effect on channel gating, we next transferred the IVS3–S4 linker together with the entire S3 transmembrane helix into the first repeat ($Ca_V1.1e$–$Ca_V1.1e$-$3L_I$). Recording currents from myotubes expressing this construct showed that the voltage dependence of activation ($V_{1/2}$ = 12.4 ± 1.4 mV; P < 0.0001) was only marginally right-shifted compared with the starting construct $Ca_V1.1e$ (Fig. 2 E) but still more than −20 mV apart from $Ca_V1.1a$ (P < 0.0001). This indicates that in the context of the I VSD D4–R1/R2 interactions are not critically involved in voltage sensor movement.
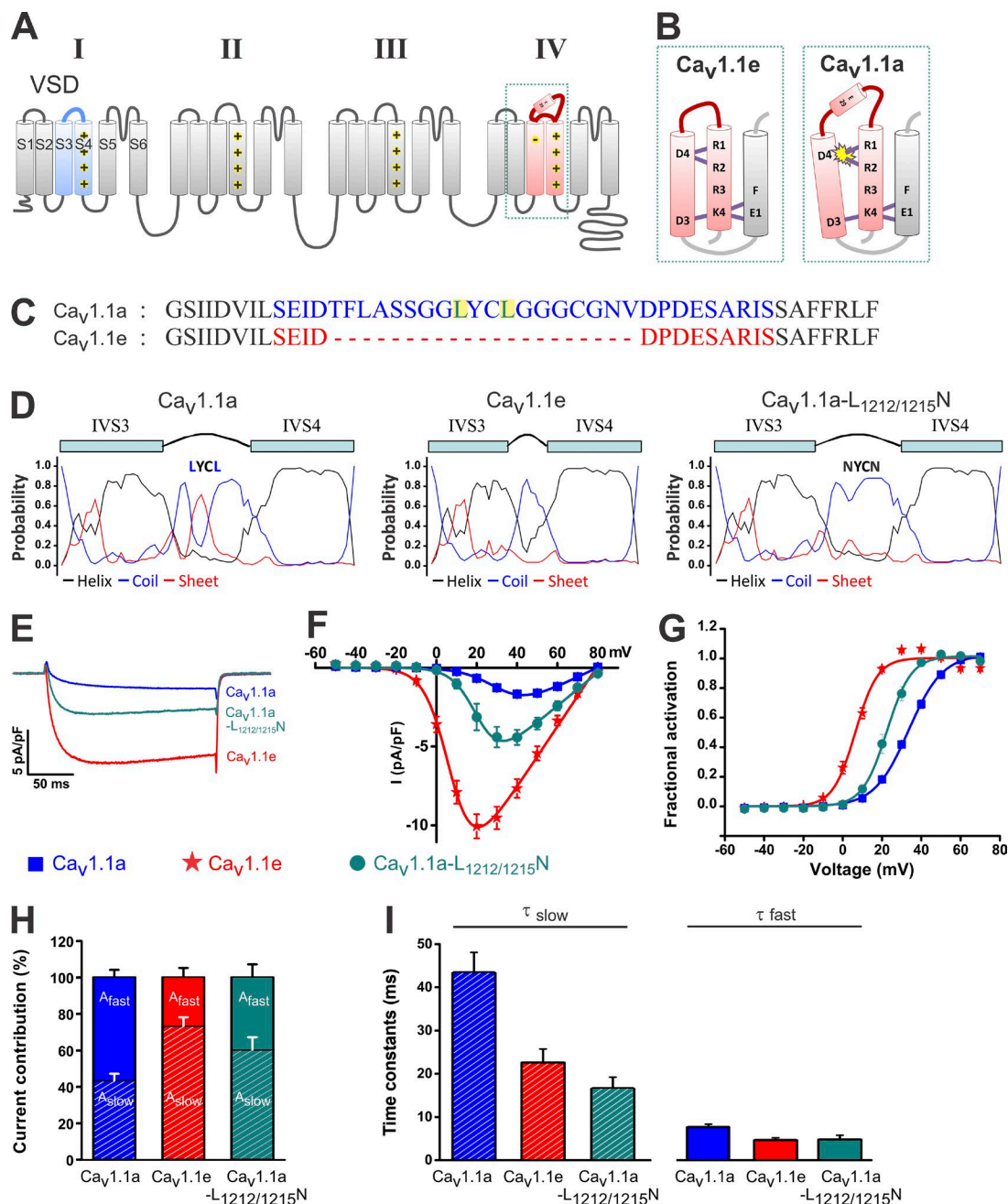
Structural determinants of $Ca_V1.1$ gating | Tuluc et al.

Figure 1. **The S3–S4 linker structure in the IV VSD controls voltage sensitivity and current density of $Ca_V1.1a$.** (A) Transmembrane topology of $Ca_V1.1$ indicating the four homologous repeats (I–IV) with six transmembrane helices (S1–S6) each. The alternatively spliced IVS3–S4 linker of the adult $Ca_V1.1a$ splice variant containing exon 29 is depicted as a barrel, whereas the embryonic $Ca_V1.1e$ splice variant lacking exon 29 is a line. (B) Model describing the role of the S3–S4 linker in controlling the interaction of R1 and R2 in IVS4 with the D4 countercharge in IVS3. (C) Sequence of the IVS3–S4 linkers of $Ca_V1.1a$ (blue) and $Ca_V1.1e$ (red). The two leucines mutated to asparagines are highlighted in yellow. (D) Secondary structure prediction of the IV VSD shows an increased probability of β-sheet in the IVS3–S4 linker of $Ca_V1.1a$ that is missing in $Ca_V1.1e$. Note that the mutation of two leucines (L1212N and L1215N) abolishes the predicted structure. (E) Representative calcium currents at maximal activation of $Ca_V1.1a$, $Ca_V1.1e$, and $Ca_V1.1e-L_{1212/1215}N$. (F and G) I/V curves and the fractional activation plot show large differences in current density and voltage sensitivity between $Ca_V1.1e$ and $Ca_V1.1a$ and intermediate values for $Ca_V1.1e-L_{1212/1215}N$. (H) Bar graphs showing the fractions of the fast and slow components of the double-exponential function fitting the raising phase of calcium currents. (I) Time constants of fast and slow activation components. Data in graphs represent mean ± SEM. Numerical values, number of samples, and statistical significance are reported in Tables 1 and 2.
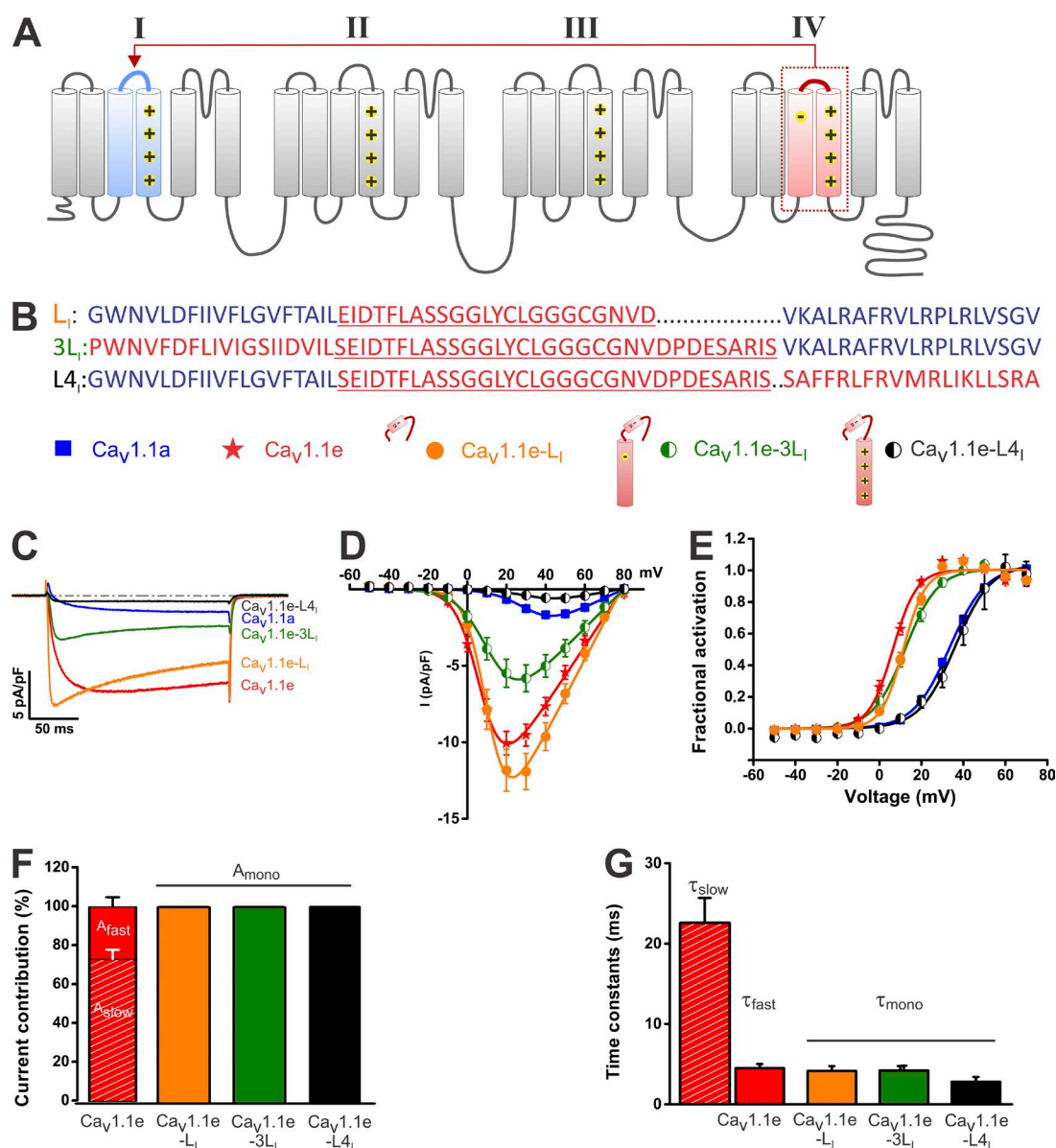
Figure 2. Control of voltage sensitivity and current amplitude can be transferred from the IV to the I VSD. (A) Transmembrane topology of $Ca_V1.1$ indicating the segments transposed from the IV to the I VSD. (B) Amino acid sequence of S3, S3–S4 linker (underlined), and S4 in the I repeat. Blue represents sequences from the I repeat and red from the IV repeat. (C) Representative calcium currents at maximal activation of $Ca_V1.1a$, $Ca_V1.1e$, $Ca_V1.1e-L_I$, $Ca_V1.1e-3L_I$, and $Ca_V1.1e-L4_I$. (D) I/V curves show that the current density is strongly reduced in $Ca_V1.1e-L4_I$ but not in the other chimeras. (E) Fractional activation plots show that only for $Ca_V1.1e-L4_I$ is the voltage sensitivity right-shifted to a similar extent as in $Ca_V1.1a$. (F) The activation kinetics of all chimeras is best described by one exponential function unlike the activation kinetics of the parent $Ca_V1.1e$ channel. (G) The time constants of the single activation component of all chimeras resemble the fast component of $Ca_V1.1e$. Data in graphs represent mean ± SEM. Numerical values, number of samples, and statistical significance are reported in Tables 1 and 2.

Finally, we transferred the IVS3–S4 linker together with the transmembrane helix S4 into the corresponding position of the I repeat ($Ca_V1.1e-L4_I$). If the proposed D4–R1/R2 interaction depends on the specific properties of S4 from the IV VSD, then transferring it into the I VSD, which lacks D4, might impede the voltage sensor movement and consequently revert the current properties of $Ca_V1.1e$ back to those of $Ca_V1.1a$. Indeed, the currents of this chimera ($Ca_V1.1e-L4_I$) were

small and activated only at much depolarized potentials (Fig. 2, C–E; and Table 1). The small current density of $Ca_V1.1e-L4_I$, ($0.6 ± 0.1$ pA/pF) and the right-shifted voltage dependence of activation ($V_{1/2} = 36.4 ± 3.1$ mV) resembled those of $Ca_V1.1a$ ($P = 0.5$), demonstrating that the limiting effects of the IV VSD can be fully transferred to the first repeat by transplanting the IVS3–S4 linker plus the adjacent IVS4 helix. The reduced current density was not caused by reduced functional membrane

Structural determinants of $Ca_V1.1$ gating | Tuluc et al.

incorporation of $Ca_V1.1e-L4_I$ channels, as the amplitude of the depolarization-induced calcium transients was similar to that of $Ca_V1.1a$ channels (not depicted).

Interestingly, the repeat IV to repeat I chimeras also affected the current kinetics. Whereas both wild-type splice variants ($Ca_V1.1a$ and $Ca_V1.1e$) are slowly activating and activation of both is composed of a slow and a fast component, all three tested IV to I chimeras were rapidly activating. Their activating phase could be fitted with a single exponential function with the activation time constants resembling the fast component of the starting construct $Ca_V1.1e$ (Fig. 2, F and G; and Table 2). The fact that the changes in activation kinetics, seen with all IV to I chimeras, do not parallel the changes in voltage dependence of activation, which was seen only in $Ca_V1.1e-L4_I$, indicates that these activation properties are determined by independent channel structures.

Insertion of $Ca_V1.2$ sequences into the I VSD alters current kinetics without affecting voltage dependence of activation of both $Ca_V1.1$ splice variants

Previously, it has been shown that the specific slow activation kinetics of the skeletal muscle $Ca_V1.1$ can be transferred to the cardiac/neuronal $Ca_V1.2$ isoform by replacing the IS3 helix plus the IS3–S4 linker in $Ca_V1.2$ with those of $Ca_V1.1$ (Nakai et al., 1994). The opposite changes observed in all of our IV to I chimeras corroborate the importance of IS3, the IS3–S4 linker, and IS4 in determining activation kinetics of $Ca_V1.1$ channels. To examine whether determination of activation kinetics and voltage sensitivity are linked or independent of each other, we generated chimeras in which IS3 and the IS3–S4 linker of both $Ca_V1.1$ splice variants were replaced by the corresponding sequences of the rapidly activating $Ca_V1.2$ channel isoforms ($Ca_V1.1a-CS_I$ and $Ca_V1.1e-CS_I$; Fig. 3, A and B). Indeed, this sequence exchange conferred fast ($Ca_V1.2$ like) activation kinetics onto $Ca_V1.1a$ as well as onto $Ca_V1.1e$ (Fig. 3 C and Table 2). Similar to the changes observed in the IV to I chimeras (compare with Fig. 2 [F and G]), both $Ca_V1.1a-CS_I$ and $Ca_V1.1e-CS_I$ displayed a single activation component equal to or faster than the fast activation component of the starting constructs $Ca_V1.1a$ ($P < 0.0001$) and $Ca_V1.1e$ ($P = 0.6$; Fig. 3, F and G; and Table 2). Importantly, the changes in activation kinetics were not accompanied by significant changes in voltage dependence of activation or of current density (Fig. 3, D and E). Although, both $Ca_V1.1a-CS_I$ and $Ca_V1.1e-CS_I$ activated rapidly, the ∼30-mV difference in voltage dependence of activation between the two $Ca_V1.1$ splice variants was still maintained (Table 1).

Transferring sequences from the I to the IV VSD modulates voltage dependence but not kinetics of activation

So far the results of this study are consistent with the notion that in $Ca_V1.1$ channels the I VSD controls mainly activation kinetics, whereas the IV VSD controls voltage dependence of activation and current density. Consequently, the individual VSDs of Ca_V1 channels appear to be functionally and structurally distinct modules, and at least for the voltage sensitivity this characteristic can be transferred between the repeats. If this is also the case for the kinetic properties, slow, two-component activation kinetics may be transferrable from the I to the IV VSD. To test this possibility, we chose as starting construct the chimera $Ca_V1.1e-L_I$ (Fig. 2 B) because it conducts sizeable calcium currents with fast, single-component activation kinetics (compare Fig. 2). Then we exchanged the corresponding sequences in repeat IV with the IS3–S4 linker alone ($Ca_V1.1e-L_I-L_{IV}$) or together with the IS3 helix ($Ca_V1.1e-L_I-3L_{IV}$), with the IS4 helix ($Ca_V1.1e-L_I-L4_{IV}$), or with both IS3 and IS4 helices ($Ca_V1.1e-L_I-3L4_{IV}$) of repeat I (Fig. 4, A and B). If any one of these I VSD sequences independently determines the characteristic skeletal muscle-like activation kinetics, we would expect chimeric channels to activate slowly with the activation kinetics described by a two-component exponential function like $Ca_V1.1e$ or $Ca_V1.1a$.

The voltage sensitivities and current amplitudes of these constructs were rather diverse and occupied the full range between those of $Ca_V1.1a$ and $Ca_V1.1e$ (Fig. 4, C–E; and Table 1). Interestingly, inserting the IS3–S4 linker into the IV repeat ($Ca_V1.1e-L_I-L_{IV}$) reduced voltage sensitivity ($V_{1/2} = 21.2$ mV) and current density to intermediate levels (7.0 pA/pF). The characteristics of $Ca_V1.1e-L_I-L_{IV}$ were very similar to those reported above for the $Ca_V1.1a-L_{1212/1215}N$ (compare with Fig. 2 [D and E] and Table 1). Apparently, either mutating the IVS3–S4 linker or replacing it by the corresponding linker of repeat I shifts the voltage dependence of activation to a similar degree, although in opposite directions. Thus, both alterations in the IVS3–S4 linker partially reproduce the effect of alternative splicing of exon 29 (see also Fig. S1). Inserting IS3 plus the IS3–S4 linker into the IV repeat ($Ca_V1.1e-L_I-3L_{IV}$) resulted in a current with small amplitude (2.1 pA/pF) and a right-shifted voltage dependence of activation ($V_{1/2} = 36.1$ mV), as expected for an S3 helix lacking D4. Both $V_{1/2}$ and current amplitude of this construct $Ca_V1.1e-L_I-3L_{IV}$ were equal to those of $Ca_V1.1a$ ($P = 0.4$, $P = 0.3$). In contrast, insertion of the IS3–S4 linker plus IS4 into the IV repeat ($Ca_V1.1e-L_I-L4_{IV}$) resulted in currents with voltage dependence and current density like $Ca_V1.1e$ ($V_{1/2} = 5.2$ mV, $P = 0.4$; $I_{peak} = 9.6$ pA/pF, $P = 0.5$). Apparently, with a heterologous S4 segment from the I repeat, the IV VSD is no longer subject to modulation by D4 and the S3–S4 linker. Similarly, insertion of the entire sequence including IS3, the IS3–S4 linker, and IS4 ($Ca_V1.1e-L_I-3L4_{IV}$) did not change either voltage dependence of activation or the current amplitude ($V_{1/2} = 10.6$ mV, $I_{peak} = 8.7$ pA/pF), suggesting that this module of the I
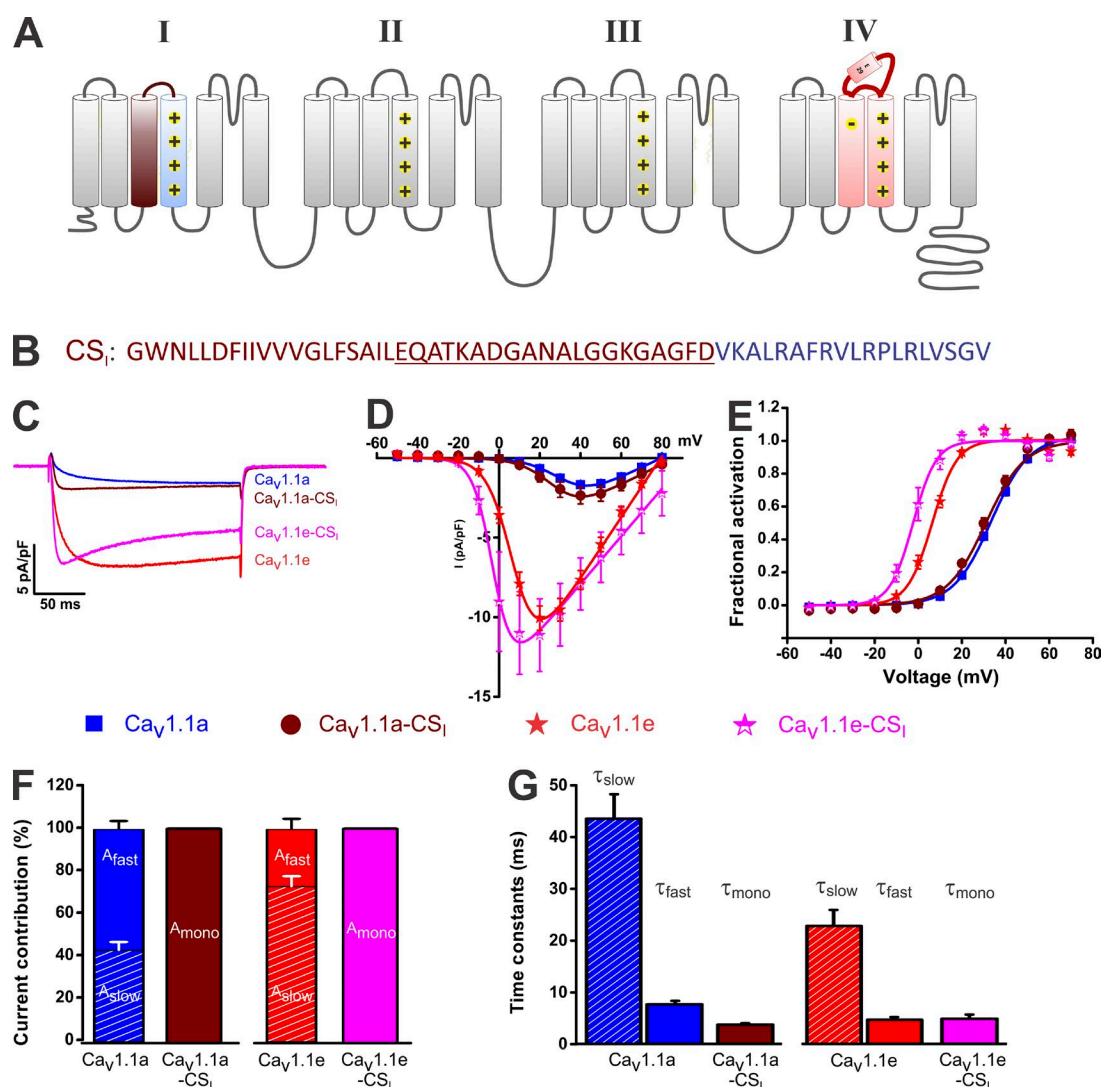
Figure 3. **Insertion of IS3 with the IS3–S4 linker of Ca$_V$1.2 into the I VSD of Ca$_V$1.1a and Ca$_V$1.1e alters kinetics but not the voltage dependence or amplitude.** (A) Transmembrane topology of Ca$_V$1.1 indicating the insertion of the Ca$_V$1.2 IS3 helix and the IS3–S4 linker (brown) into the corresponding regions of Ca$_V$1.1. (B) Amino acid sequence of cardiac S3, S3–S4 linker (brown), and skeletal S4 (blue) in the I repeat VSD. (C) Representative calcium currents at maximal activation of Ca$_V$1.1a, Ca$_V$1.1e, Ca$_V$1.1a-CS$_I$, and Ca$_V$1.1e-CS$_I$. (D and E) I/V curves (D) and fractional activation plots (E) show that neither current density nor voltage sensitivity is significantly affected by insertion of the cardiac IS3 and IS3–S4 linker in Ca$_V$1.1a or Ca$_V$1.1e. (F) Transferring the Ca$_V$1.2 IS3 helix and IS3–S4 linker into Ca$_V$1.1 gives rise to currents with the activation phase described by a single exponential function. (G) The time constants of the single activation component of Ca$_V$1.1a-CS$_I$ and Ca$_V$1.1e-CS$_I$ resemble the fast components of Ca$_V$1.1a and Ca$_V$1.1e. Data in graphs represent mean ± SEM. Numerical values, number of samples, and statistical significance are reported in Tables 1 and 2.

VSD is functionally equivalent to that of the IV VSD without exon 29 (Ca$_V$1.1e; P = 0.4, P = 0.4).

Although voltage dependence of activation and current density were differentially affected by these I to IV sequence exchanges, none of these chimeras reproduced the slow, two-component activation kinetics of the wild-type Ca$_V$1.1 channels (Table 2). All I to IV chimeras activated rapidly, activation could be fit with a single exponential, and time constants were comparable with that of the starting chimera Ca$_V$1.1e-L$_I$ (Table 1). Apparently, the activation kinetics determined by the I VSD cannot be overcome by any of the tested insertions of repeat I sequences into the IV repeat.

DISCUSSION

Previously, we demonstrated that in the IV VSD the interaction between D4 (D1196) in IVS3 and R1 and R2 in IVS4 are critical for the voltage sensitivity of Ca$_V$1.1 calcium currents and that the alternatively spliced IVS3–S4 linker modulates this critical interaction so that the voltage dependence of current activation in the
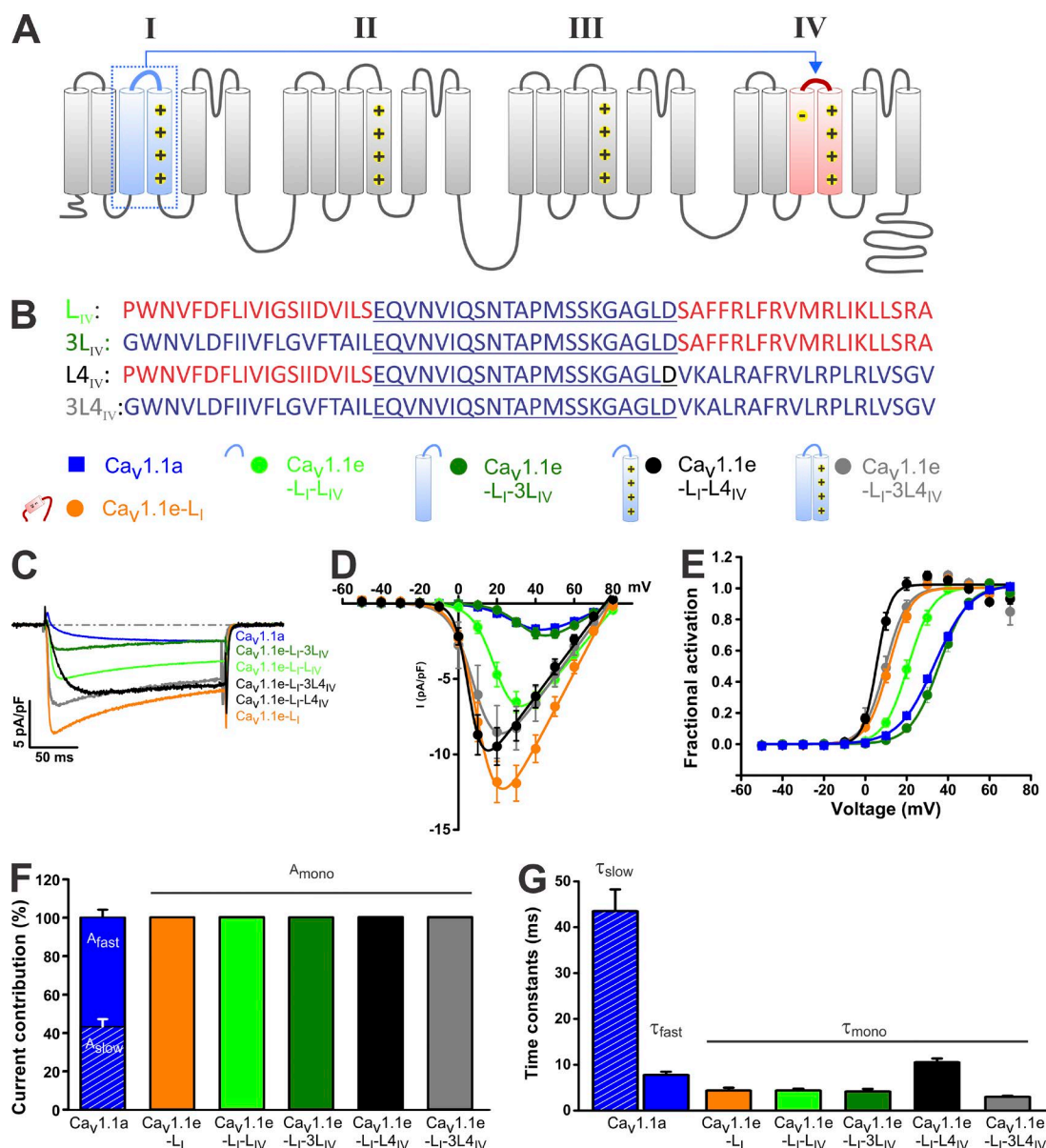
Figure 4. Transferring S3 and the S3–S4 linker from the I to IV VSD modulates voltage dependence and amplitude but not kinetics of activation. (A) The transmembrane topology model of $Ca_V1.1$ indicating the segments transposed from the I to the IV VSD (red). These chimeras are based on $Ca_V1.1e-L_I$ containing the IVS3 linker in the I VSD and displaying fast, single-component activation kinetics. (B) Amino acid sequence of S3, S3–S4 linker (underlined), and S4 in the IV repeat. Red depicts sequences from the IV repeat, whereas blue depicts sequences from the I repeat. (C) Representative calcium currents at maximal activation of $Ca_V1.1a$, $Ca_V1.1e-L_I$, $Ca_V1.1e-L_I-L_{IV}$, $Ca_V1.1e-L_I-3L_{IV}$, $Ca_V1.1e-L_I-L4_{IV}$, and $Ca_V1.1e-L_I-3L4_{IV}$. (D) I/V curves show that the current density is strongly reduced upon transfer of the IS3 plus the IS3–S4 linker to the IV VSD ($Ca_V1.1e-L_I-3L_{IV}$) and moderately reduced upon transfer of the IS3–S4 linker alone ($Ca_V1.1e-L_I-L_{IV}$). (E) Voltage dependence of activation shows that transferring S3 plus the S3–S4 linker from the I to the IV repeat converts the voltage sensitivity of $Ca_V1.1e-L_I$ to $Ca_V1.1a$. (F) All chimeras activated with single-component kinetics, indicating that transferring sequences from the I to the IV VSD cannot reproduce slow current activation of $Ca_V1.1a$. (G) Time constants of the single activation components of these chimeras resemble kinetics of the fast component of $Ca_V1.1a$. Data in graphs represent mean ± SEM. Numerical values, number of samples, and statistical significance are reported in Tables 1 and 2.

adult splice variant $Ca_V1.1a$ is right-shifted by ∼30 mV compared with the embryonic $Ca_V1.1e$ splice variant lacking exon 29 (Tuluc et al., 2016). Using point mutations and multiple channel chimeras in which we swapped sequence domains between the I and the IV VSD of $Ca_V1.1$, we demonstrate here that (a) mutation or substitution of the IVS3–S4 linker modulates the voltage sensitivity in the context of the IV VSD, whereas the IVS3–S4 linker has no modulatory activity of its own when inserted into the I VSD; (b) the transmembrane helix IVS4 is functionally distinct from IS4 in that it specifically requires the interaction with its corresponding

IVS3 (containing D4), whereas IVS3 functions in both VSDs. Moreover, by analyzing current kinetics of the chimeras, we demonstrate that (c) IS3, the IS3–S4 linker, and IS4 are all necessary for slow, skeletal muscle type activation, but neither separately nor combined are these domains sufficient to effect slow activation in the context of the IV VSD.

The Ca$_V$1.1 IVS3–S4 linker specifically regulates voltage sensing in the IV VSD

Mutations in Ca$_V$1.1a expected to break the structure and alter the hydrophobicity of the IVS3–S4 linker improved the voltage sensitivity and increased the current density of Ca$_V$1.1a. Although this mutation did not completely reverse the limiting effect of exon 29 inclusion, this result strongly supports the notion that the structural integrity of the IVS3–S4 linker is important for its role in determining the characteristic gating properties of Ca$_V$1.1a. As mutation of the two leucines alters both the predicted structure (helix or β-sheet) and the hydrophobicity of the IVS3–S4 linker, we cannot say which of these properties is critical for modulating the voltage sensor. However, because the original length of the linker was maintained, we can exclude the alternative explanation that simply the length of the IVS3–S4 linker determines the voltage sensitivity of Ca$_V$ channels. This is different from the situation in K$_V$ channels where the lengths of the loop alters the transition of the VSD (Priest et al., 2013) and from Ca$_V$1.2 channel splice variants where the length of the IVS3–S4 linker correlates with the voltage dependence of activation (Tang et al., 2004). Given the importance of the structure of the IVS3–S4 linker, this domain might be sufficient to perturb the movement of any VSD and thus cause the loss of voltage sensitivity. However, when inserted into the VSD of the I repeat, the IVS3–S4 linker had no effect on voltage sensitivity or current amplitude. This clearly demonstrates that the structural features of exon 29 are not sufficient to curtail voltage sensitivity in any VSD. Apparently, other unique features of the IV VSD are necessary for the IVS3–S4 linker to modulate the current properties.

The IV VSD but not the I VSD requires the D4–R1/R2 interaction

When we examined which additional structural domains are required to transfer right-shifted voltage sensitivity from the IV to the I VSD, it turned out that IVS4, but not IVS3, is needed in addition to the IVS3–S4 linker to precisely recapitulate the gating properties of Ca$_V$1.1a. In the reverse set of chimeras, IS3 plus the IS3–S4 linker, but not the IS3–S4 linker plus IS4, right-shifted the voltage sensitivity. Both chimeras that resulted in right-shifted $V_{1/2}$ combine the S3 from the I VSD with S4 from the IV VSD, suggesting that this mis-match is the primary cause of the observed loss of voltage sensitivity. This mechanism is independent of exon 29 in the IVS3–S4 linker, as it also occurs with the IS3–S4 linker, which otherwise supports normal voltage sensing in both repeats. Interestingly, the opposite mismatch, S3 from the IV and S4 from the I VSD, did not perturb voltage sensing. This demonstrates that IVS4 specifically requires IVS3 for normal voltage sensitivity, but IVS3 functions perfectly well with the S4 helices from either VSDs.

Together with our previous discovery of the essential role of an intramolecular interaction of aspartate D4 in the IVS3 helix with the two outermost arginines (R1 and R2) in IVS4 (Tuluc et al., 2016), the current results suggest the following model for the regulation of voltage sensitivity in the Ca$_V$1.1 splice variants (Fig. 5). The S4 helix of the IV VSD is different from that of the I VSD in that it specifically and critically requires additional transient interactions with D4 in the IVS3 helix for effective voltage sensing. This interaction most likely facilitates the final transition and stabilization of the VSD in the activated state (Tuluc et al., 2016). At present, we do not know what exactly constitutes this difference in IVS4, but combining it with S3 helices lacking D4 consistently results in loss of voltage sensitivity. Although D4 in the S3 helix is of critical importance for the function of IVS4, in combination with IS4, the presence of D4 does not affect the voltage sensitivity. Thus, D4 functions exclusively as an essential partner for IVS4.

The dependence of the voltage sensor on this additional intramolecular interaction near the extracellular side of the IV VSD creates a mechanism enabling the modulation of the voltage dependence of activation by alternative splicing of the linker connecting the two participating transmembrane helices. When the relative position of IVS3 and IVS4 is altered by insertion of exon 29, voltage sensitivity is right-shifted by ∼30 mV. Consistent with this notion, mutation of exon 29 or replacing the entire linker with that of repeat I caused partial shifts in voltage dependence of activation. This also shows that this modulatory mechanism does not necessarily function as an all or none switch but can function in a graded manner. Our previous structure-function analysis of the IVS3–IVS4 interactions predicted the participation of multiple transient hydrogen bonds between D4 and the two outermost arginines R1 and R2 in the last transition and the subsequent stabilization of the voltage sensor in the activated state. Therefore, it is intriguing to speculate that the partial shift in voltage sensitivity observed here might be caused by the selective loss of one or two of these bonds while others might remain intact. A critical role of interaction between S3 and S4 helices in controlling the energetics of voltage sensor activation by stabilizing the activated state has also been shown for the Shaker K$^+$ channel (Xu et al., 2013).
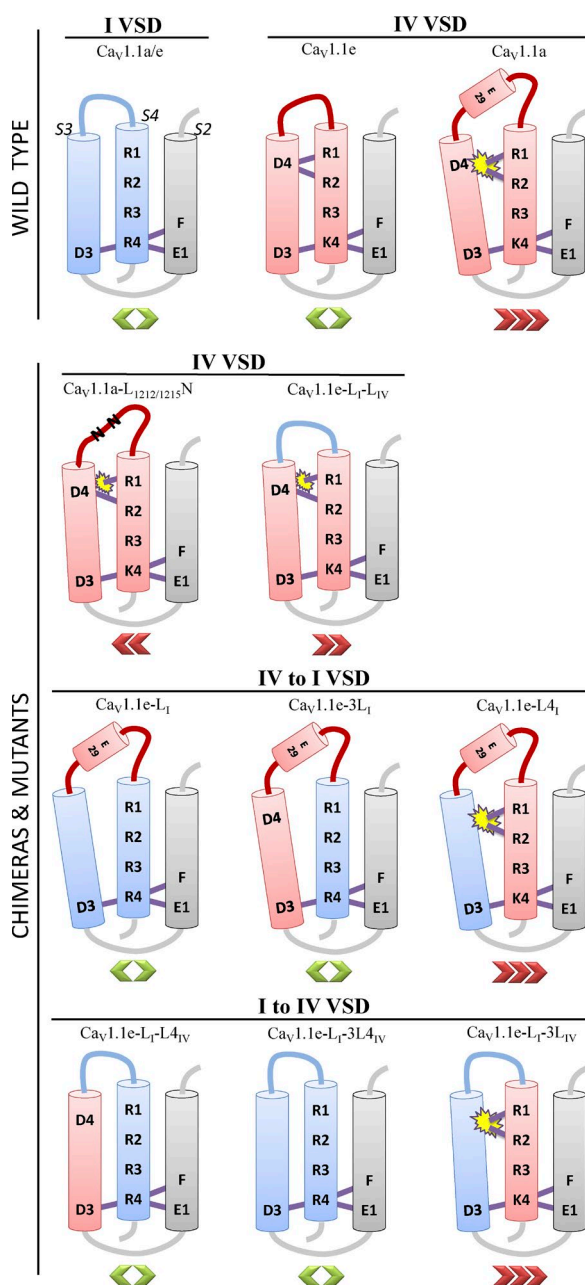
Structural determinants of Ca$_V$1.1 gating | Tuluc et al.

Figure 5. **Voltage-gating model of the I and IV VSDs of wild-type and mutated Ca_V1.1 channels.** The three cylinders depict the transmembrane segments S2, S3, and S4 with critical amino acids indicated in single letter code. F, E1, and D3 represent the charge transfer center through which the positively charged amino acids of the S4 segment move in response to depolarization. Depicted is the activated state with the innermost positive charge of IVS4 (K4) occupying the charge transfer center. Purple bars represent proposed hydrogen bonds. The IV VSD (red) but not the I VSD (blue) contains an additional counter charge D4 in S3 (Tuluc et al., 2016). Any channel construct containing IVS4 in combination with IS3 (without D4; Ca_V1.1e-L4_I and Ca_V1.1e-L_I-3L_IV) or in which the IVS3 segment (containing D4) is displaced from IVS4 by insertion of exon 29 (Ca_V1.1e) or the heterologous IS3–S4 linker (Ca_V1.1e-L_I-L_IV) results in a right-shifted voltage dependence of activation (red chevrons). Conversely, a mutation that relaxes the structure and reduces the hydrophobicity of exon 29 (Ca_V1.1e-L_{1212/1215}N) partially

The kinetic properties of Ca_V1.1 activation are determined by the I VSD independently of the regulation of voltage sensitivity

Kinetic analysis of our channel chimeras is consistent with earlier results suggesting that the characteristics of Ca_V1.1 activation—very slow time course composed of two kinetic components—are determined by the VSD of the I repeat (Nakai et al., 1994). Transfer of the IS3 helix and the IS3–S4 linker from Ca_V1.2 into Ca_V1.1a and Ca_V1.1e gave rise to channel chimeras with fast, cardiac-like activation kinetics. But also any insertion into the I VSD of sequences from the IV VSD of Ca_V1.1 changed the activation kinetics in a similar way. This indicates that the changes of channel kinetics in the Ca_V1.1-Ca_V1.2 chimeras were not caused by a gain of Ca_V1.2 function but by a loss of the specific Ca_V1.1 function. Apparently, the specific kinetic properties of the I VSD of Ca_V1.1 are highly sensitive to any changes, be it from a different channel isoform or from a different VSD of the same channel isoform. This notion is further supported by the finding that, in contrast to the voltage dependence of activation, kinetic properties could not be transferred from one to another VSD of the same channel. This is surprising considering that transfer of the same sequences from Ca_V1.1 to Ca_V1.2 was sufficient to confer slow activation onto the cardiac/neuronal channel (Nakai et al., 1994). In contrast, this discrepancy further emphasizes the substantial difference of the VSD within a Ca_V1 channel. Apparently, the I VSDs of Ca_V1.1 and Ca_V1.2 share more functional similarities with one another than the I and IV VSD of Ca_V1.1.

Together, these results show that Ca_V1.1 is organized in a modular way so that specific VSDs control distinct properties of L-type calcium current activation. Distinct contributions of the different VSDs to channel gating have previously been described for Na_V1.2a VSDs transplanted into the K_V2.1 channel (Bosmans et al., 2008). In our study, we demonstrate that repeat I is responsible for determining the kinetics of activation, whereas repeat IV is responsible for determining the voltage dependence of activation and, at least in part, the current density. Accordingly, the two aspects of activation properties are not linked to each other and can be modulated separately. Alternative splicing of exon 29 in the IV VSD does not affect current kinetics, and conversely, acceleration of activation kinetics by inser-

recovers voltage sensitivity. However, there is no requirement of D4–R1/R2 interactions in the absence of IVS4, as chimeras containing IVS3 in combination with IS4 gate equally well with and without the IVS3–S4 linker (Ca_V1.1e-3L_I and Ca_V1.1e-L_I-L4_IV; green chevrons). Because insertion of the IVS3–S4 linker in the I VSD (Ca_V1.1e-L_I) does not alter voltage sensitivity, this extracellular loop and its alternative splicing have no modulatory potential on VSDs lacking the D4–R1/R2 interactions.

tion of heterologous sequences into the I VSD does not correlate with changes in the voltage dependence of activation. Moreover, also the molecular mechanisms for the control of voltage dependence and kinetics of activation are different. Regulation of voltage sensitivity is accomplished by a structurally well-defined mechanism entailing IVS3, the IVS3–S4 linker, and IVS4. It can be transferred from one VSD to another, suggesting that it basically involves the control of S4 gating charge movement through the IV VSD. In contrast, control of current kinetics cannot be transferred from one to another VSD, suggesting that it does not function by controlling the speed of S4 movement in the VSD. Likely it involves structures outside the I VSD that accomplish the transduction of the VSD movement to opening of the channel pore.

In voltage-gated sodium channels, distinct contributions of the four VSDs to activation and inactivation have long been known (reviewed in Ahern et al. [2016]). In this channel, the IV VSD is distinct from VSDs I–III in that its movement is not necessary for channel activation but is a prerequisite to inactivation. Recently, voltage-clamp fluorometry was applied to analyze the individual contributions of the four VSDs of the $Ca_V1.2$ channel (Pantazis et al., 2014). Interestingly, in this channel, the voltage sensitivity and activation kinetics of the VSD II and III best resembled the ionic current properties, whereas VSD I contributed little and VSD IV not at all to channel gating. Our data agree with the notion of a heterogeneity of the four VSDs in Ca_V channels. However, they also suggest that in $Ca_V1.1$—the primary function of which is in activating RyR1—the specific roles of the individual VSDs are distinct from those in $Ca_V1.2$. Notably, the observation that unique features of the IVS3–S4 linker and IVS4 control voltage sensitivity in the IV VSD and, when transplanted, also in the I VSD, indicate that in $Ca_V1.1$ both of these VSD are essential for channel gating.

Considering this evidence in support of a modular organization of the $Ca_V1.1$ calcium channel, it will be of interest to also unravel the role of the remaining two VSDs of the II and III repeats in $Ca_V1.1$. In addition to their involvement in channel gating, these repeats are likely important in the activation of EC coupling. Because EC coupling activates with faster kinetics and at left-sifted voltages compared with $Ca_V1.1a$ current activation, we assume that the I and IV VSD are not involved in this signaling process at all, but exclusively function in channel gating. Sequence similarities between the I and the III and between the II and the IV VSD of Ca_V channels suggest a twofold symmetry of the channel. The distinct voltage-sensing mechanisms reported here for VSDs I and IV may be replicated in VSDs III and II, respectively. However, this hypothesis remains to be tested in future studies.

REFERENCES

Ahern, C.A., J. Payandeh, F. Bosmans, and B. Chanda. 2016. The hitchhiker's guide to the voltage-gated sodium channel galaxy. *J. Gen. Physiol.* 147:1–24. http://dx.doi.org/10.1085/jgp.201511492

Armstrong, C.M., F.M. Bezanilla, and P. Horowicz. 1972. Twitches in the presence of ethylene glycol bis(β-aminoethyl ether)-*N,N′*-tetracetic acid. *Biochim. Biophys. Acta.* 267:605–608. http://dx.doi.org/10.1016/0005-2728(72)90194-6

Avila, G., and R.T. Dirksen. 2000. Functional impact of the ryanodine receptor on the skeletal muscle L-type Ca^{2+} channel. *J. Gen. Physiol.* 115:467–480. http://dx.doi.org/10.1085/jgp.115.4.467

Benedetti, B., P. Tuluc, V. Mastrolia, C. Dlaska, and B.E. Flucher. 2015. Physiological and pharmacological modulation of the embryonic skeletal muscle calcium channel splice variant $Ca_V1.1e$. *Biophys. J.* 108:1072–1080. http://dx.doi.org/10.1016/j.bpj.2015.01.026

Bosmans, F., M.F. Martin-Eauclaire, and K.J. Swartz. 2008. Deconstructing voltage sensor function and pharmacology in sodium channels. *Nature.* 456:202–208. http://dx.doi.org/10.1038/nature07473

Caffrey, J.M. 1994. Kinetic properties of skeletal-muscle-like high-threshold calcium currents in a non-fusing muscle cell line. *Pflugers Arch.* 427:277–288. http://dx.doi.org/10.1007/BF00374535

Catterall, W.A. 2011. Voltage-gated calcium channels. *Cold Spring Harb. Perspect. Biol.* 3:a003947. http://dx.doi.org/10.1101/cshperspect.a003947

Combet, C., C. Blanchet, C. Geourjon, and G. Deléage. 2000. NPS@: network protein sequence analysis. *Trends Biochem. Sci.* 25:147–150. http://dx.doi.org/10.1016/S0968-0004(99)01540-6

Flucher, B.E., N. Kasielke, U. Gerster, B. Neuhuber, and M. Grabner. 2000. Insertion of the full-length calcium channel α_{1S} subunit into triads of skeletal muscle in vitro. *FEBS Lett.* 474:93–98. http://dx.doi.org/10.1016/S0014-5793(00)01583-0

Flucher, B.E., G.J. Obermair, P. Tuluc, J. Schredelseker, G. Kern, and M. Grabner. 2005. The role of auxiliary dihydropyridine receptor subunits in muscle. *J. Muscle Res. Cell Motil.* 26:1–6. http://dx.doi.org/10.1007/s10974-005-9000-2

Gur, M., R. Kahn, I. Karbat, N. Regev, J. Wang, W.A. Catterall, D. Gordon, and M. Gurevitz. 2011. Elucidation of the molecular basis of selective recognition uncovers the interaction site for the core domain of scorpion α-toxins on sodium channels. *J. Biol. Chem.* 286:35209–35217. http://dx.doi.org/10.1074/jbc.M111.259507

Kugler, G., R.G. Weiss, B.E. Flucher, and M. Grabner. 2004. Structural requirements of the dihydropyridine receptor α_{1S} II-III loop for skeletal-type excitation-contraction coupling. *J. Biol. Chem.* 279:4721–4728. http://dx.doi.org/10.1074/jbc.M307538200

Lipscombe, D., A. Andrade, and S.E. Allen. 2013. Alternative splicing: functional diversity among voltage-gated calcium channels and behavioral consequences. *Biochim. Biophys. Acta.* 1828:1522–1529. http://dx.doi.org/10.1016/j.bbamem.2012.09.018

Melzer, W., A. Herrmann-Frank, and H.C. Lüttgau. 1995. The role of Ca^{2+} ions in excitation-contraction coupling of skeletal muscle fibres. *Biochim. Biophys. Acta.* 1241:59–116. http://dx.doi.org/10.1016/0304-4157(94)00014-5

Nakai, J., B.A. Adams, K. Imoto, and K.G. Beam. 1994. Critical roles of the S3 segment and S3-S4 linker of repeat I in activation of L-type calcium channels. *Proc. Natl. Acad. Sci. USA.* 91:1014–1018. http://dx.doi.org/10.1073/pnas.91.3.1014

Obermair, G.J., G. Kugler, S. Baumgartner, P. Tuluc, M. Grabner, and B.E. Flucher. 2005. The Ca^{2+} channel $\alpha_2\delta$-1 subunit determines Ca^{2+} current kinetics in skeletal muscle but not targeting of α_{1S} or excitation-contraction coupling. *J. Biol. Chem.* 280:2229–2237. http://dx.doi.org/10.1074/jbc.M411501200

Pantazis, A., N. Savalli, D. Sigg, A. Neely, and R. Olcese. 2014. Functional heterogeneity of the four voltage sensors of a human L-type calcium channel. *Proc. Natl. Acad. Sci. USA.* 111:18381–18386. http://dx.doi.org/10.1073/pnas.1411127112

Powell, J.A., L. Petherbridge, and B.E. Flucher. 1996. Formation of triads without the dihydropyridine receptor alpha subunits in cell lines from dysgenic skeletal muscle. *J. Cell Biol.* 134:375–387. http://dx.doi.org/10.1083/jcb.134.2.375

Priest, M.F., J.J. Lacroix, C.A. Villalba-Galea, and F. Bezanilla. 2013. S3-S4 linker length modulates the relaxed state of a voltage-gated potassium channel. *Biophys. J.* 105:2312–2322. http://dx.doi.org/10.1016/j.bpj.2013.09.053

Rios, E., and G. Brum. 1987. Involvement of dihydropyridine receptors in excitation-contraction coupling in skeletal muscle. *Nature.* 325:717–720. http://dx.doi.org/10.1038/325717a0

Santoro, M., R. Piacentini, M. Masciullo, M.L. Bianchi, A. Modoni, M.V. Podda, E. Ricci, G. Silvestri, and C. Grassi. 2014. Alternative splicing alterations of Ca^{2+} handling genes are associated with Ca^{2+} signal dysregulation in myotonic dystrophy type 1 (DM1) and type 2 (DM2) myotubes. *Neuropathol. Appl. Neurobiol.* 40:464–476. http://dx.doi.org/10.1111/nan.12076

Sultana, N., B. Dienes, A. Benedetti, P. Tuluc, P. Szentesi, M. Sztretye, J. Rainer, M.W. Hess, C. Schwarzer, G.J. Obermair, et al. 2016. Restricting calcium currents is required for correct fiber type specification in skeletal muscle. *Development.* http://dx.doi.org/10.1242/dev.129676

Tanabe, T., K.G. Beam, J.A. Powell, and S. Numa. 1988. Restoration of excitation-contraction coupling and slow calcium current in dysgenic muscle by dihydropyridine receptor complementary DNA. *Nature.* 336:134–139. http://dx.doi.org/10.1038/336134a0

Tang, Z.Z., M.C. Liang, S. Lu, D. Yu, C.Y. Yu, D.T. Yue, and T.W. Soong. 2004. Transcript scanning reveals novel and extensive splice variations in human l-type voltage-gated calcium channel, Ca$_V$1.2 α_1 subunit. *J. Biol. Chem.* 279:44335–44343. http://dx.doi.org/10.1074/jbc.M407023200

Tang, Z.Z., V. Yarotskyy, L. Wei, K. Sobczak, M. Nakamori, K. Eichinger, R.T. Moxley, R.T. Dirksen, and C.A. Thornton. 2012. Muscle weakness in myotonic dystrophy associated with misregulated splicing and altered gating of Ca$_V$1.1 calcium channel. *Hum. Mol. Genet.* 21:1312–1324. http://dx.doi.org/10.1093/hmg/ddr568

Tao, X., A. Lee, W. Limapichat, D.A. Dougherty, and R. MacKinnon. 2010. A gating charge transfer center in voltage sensors. *Science.* 328:67–73. http://dx.doi.org/10.1126/science.1185954

Tuluc, P., G. Kern, G.J. Obermair, and B.E. Flucher. 2007. Computer modeling of siRNA knockdown effects indicates an essential role of the Ca^{2+} channel $\alpha_2\delta$-1 subunit in cardiac excitation-contraction coupling. *Proc. Natl. Acad. Sci. USA.* 104:11091–11096. http://dx.doi.org/10.1073/pnas.0700577104

Tuluc, P., N. Molenda, B. Schlick, G.J. Obermair, B.E. Flucher, and K. Jurkat-Rott. 2009. A Ca$_V$1.1 Ca^{2+} channel splice variant with high conductance and voltage-sensitivity alters EC coupling in developing skeletal muscle. *Biophys. J.* 96:35–44. http://dx.doi.org/10.1016/j.bpj.2008.09.027

Tuluc, P., V. Yarov-Yarovoy, B. Benedetti, and B.E. Flucher. 2016. Molecular interactions in the voltage sensor controlling gating properties of Ca$_V$ calcium channels. *Structure.* 24:261–271. http://dx.doi.org/10.1016/j.str.2015.11.011

Wang, J., V. Yarov-Yarovoy, R. Kahn, D. Gordon, M. Gurevitz, T. Scheuer, and W.A. Catterall. 2011. Mapping the receptor site for α-scorpion toxins on a Na$^+$ channel voltage sensor. *Proc. Natl. Acad. Sci. USA.* 108:15426–15431. (published erratum appears in *Proc. Natl. Acad. Sci. USA.* 2014. 111:3645) http://dx.doi.org/10.1073/pnas.1112320108

Xu, Y., Y. Ramu, H.G. Shin, J. Yamakaze, and Z. Lu. 2013. Energetic role of the paddle motif in voltage gating of Shaker K$^+$ channels. *Nat. Struct. Mol. Biol.* 20:574–581. http://dx.doi.org/10.1038/nsmb.2535